

Provided for non-commercial research and education use.
Not for reproduction, distribution or commercial use.



This article appeared in a journal published by Elsevier. The attached copy is furnished to the author for internal non-commercial research and education use, including for instruction at the authors institution and sharing with colleagues.

Other uses, including reproduction and distribution, or selling or licensing copies, or posting to personal, institutional or third party websites are prohibited.

In most cases authors are permitted to post their version of the article (e.g. in Word or Tex form) to their personal website or institutional repository. Authors requiring further information regarding Elsevier's archiving and manuscript policies are encouraged to visit:

<http://www.elsevier.com/authorsrights>



Contents lists available at ScienceDirect

Coastal Engineering

journal homepage: www.elsevier.com/locate/coastaleng

Breaking wave-induced response of composite breakwater and liquefaction in seabed foundation

Ye Jianhong^{a,c,*}, Jeng Dongsheng^{b,c}, P.L.-F. Liu^d, A.H.C. Chan^e, Wang Ren^a, Zhu Changqi^a

^a State Key Laboratory of Geomechanics and Geotechnical Engineering, Institute of Rock and Soil Mechanics, Chinese Academy of Sciences, Wuhan 430071 China

^b Griffith School of Engineering, Griffith University, Gold Coast, Queensland 4222, Australia

^c Division of Civil Engineering, University of Dundee, Dundee DD1 4HN, UK

^d School of Civil and Environmental Engineering, Cornell University, Ithaca, NY 14853, USA

^e School of Civil Engineering, University of Birmingham, Birmingham, B15 2TT, UK

ARTICLE INFO

Article history:

Received 12 September 2011

Received in revised form 9 June 2013

Accepted 10 August 2013

Available online 17 September 2013

Keywords:

Wave–seabed–structures interaction (WSSI)

Porous seabed

Breaking wave

Biot's theory

Composite breakwater

Liquefaction of seabed

ABSTRACT

In the practice of engineering, breaking wave is much more dangerous for the stability of composite breakwater built on porous seabed than non-breaking wave in offshore area. In previous investigations or design codes, the empirical formulations generally were adopted to estimate the wave impact acting on the lateral side of caisson. The interaction between breaking wave, seabed foundation and composite breakwater is not taken into consideration. In this study, adopting the integrated numerical model PORO-WSSI 2D developed by (Ye, 2012a) and (Jeng et al., 2013), the interaction mechanism between breaking wave, seabed foundation and composite breakwater is investigated numerically. In PORO-WSSI 2D, the Volume-Averaged Reynolds Averaged Navier–Stokes (VARANS) equations govern the wave motion and the porous flow in seabed foundation and in rubble mound; and the dynamic Biot's equations (known as “*u-p*” approximation) govern the dynamic behaviors of seabed foundation and composite breakwater under breaking wave loading. Numerical analysis indicates that the turbulent energy of breaking wave is significant, and the wave impact on caisson applied by breaking wave is much greater than non-breaking wave. The composite breakwater and its seabed foundation respond to the breaking wave loading intensively. The maximum horizontal vibration magnitude of the composite breakwater is up to 5 mm; the maximum liquefaction depth in the seabed in front of the composite breakwater reaches up to 1.2 to 1.6 m. The parametric study shows that the permeability and saturation of seabed, wave height are three dominant factors for the wave-induced liquefaction in seabed foundation.

© 2013 Elsevier B.V. All rights reserved.

1. Introduction

In the recent twenty years, more and more marine structures, such as breakwater, are constructed in the offshore area to control sediment transportation condition, or to block the wave energy propagating to the inside of ports etc. However, these breakwaters built on seabed are vulnerable to the liquefaction and shear failure of seabed foundation due to the build-up of excess pore pressure or the excessive shear stress developed in seabed foundation under ocean wave loading. Therefore, the evaluation of the dynamic response of breakwaters and their seabed foundation is particularly important and necessary for coastal engineers involved in the design of marine structures in engineering. Inappropriate design and maintenance for marine structures and their seabed foundation due to incomplete understanding of the mechanism of wave–seabed–structure interaction (WSSI) could result in the collapse of breakwater. It is well known that the effect of a breaking wave on

the stability of breakwater and its seabed foundation is much more adverse than that of a non-breaking wave. When a wave with large height and long period propagates on seabed to a breakwater, the interaction between the wave and breakwater is very intensive. The wave would break, and give a very strong impact force to the breakwater. This wave impact on breakwater would be 10–50 times of that induced by a non-breaking wave (Makenna, 1997). This intensive interaction between breaking wave and breakwater would push down the breakwater; and also would make the seabed foundation under or near to the breakwater to liquefy. Therefore, the investigation of the interaction between breaking wave, seabed foundation and breakwater is significantly meaningful in the practice of engineering.

Some investigations have been conducted on the topic of wave-induced seabed dynamic response adopting the Stokes wave theory and poro-elastic Biot's theory (Biot, 1941, 1956) since the 1970s. Some analytical solutions were proposed for the wave-induced dynamic response of seabed under ocean wave loading (Cha et al., 2002; Madsen, 1978; Ulker et al., 2009; Yamamoto et al., 1978). There was no any marine structure on seabed, and the linear or nonlinear Stokes waves were used to apply dynamic force on seabed surface. Hsu and Jeng (1994) and Jeng and Hsu (1996) developed another analytical

* Corresponding author at: State Key Laboratory of Geomechanics and Geotechnical Engineering, Institute of Rock and Soil Mechanics, Chinese Academy of Sciences, Wuhan 430071, China.

E-mail address: yejianhongcas@gmail.com (Y. Jianhong).

solutions for the wave-induced dynamic response of seabed under short-crested waves loading, in which the wave reflection in front of a long breakwater was considered. However, the marine structure was simplified as a line without width and weight in their model. Similar methods are also adopted by Tsai (1995) and Tsai et al. (2000). In some numerical models, the shape of marine structures built on seabed foundation generally could be considered in the soil model (Jeng et al., 2001; Mase et al., 1994; Ulker et al., 2010). However, the effect of weight of marine structures on the internal effective stresses field in the seabed foundation, and the effect of marine structures on the wave field were not considered. Additionally, the analytical solution of wave-induced pressure based on the Stokes wave theory and Laplace's equation was widely used to apply the force on seabed surface. As a result, the wave-induced force acting on marine structures was unknown; and the dynamic response of marine structures under wave loading could not be determined in calculation. Furthermore, the porous seabed was always treated as rigid and impermeable obstacle in Stokes wave theory. Obviously, the fluid exchange between sea water and pore water in porous seabed was not taken into consideration in Stokes wave theory. Recently, some numerical models were further developed to consider the interaction between sea water and pore water in porous medium by adopting the Volume-Averaged Reynolds Averaged Navier–Stokes (VARANS) equations to govern the wave motion and the porous flow in porous medium (Huang et al., 2003; Hur et al., 2008, 2010; Lara et al., 2006; Liu et al., 1999; Shao, 2010). The continuity of pressure, velocity/flux of water at the interfaces is applied in solving the VARANS equations. Unfortunately, the stress state and the dynamic response of seabed and marine structures could not be determined using this kind of method. Therefore, the above mentioned analytical solutions and numerical models are incapable of full understanding of the mechanism of fluid–structures–seabed interaction.

Mizutani et al. (1998) and Mostafa et al. (1999) developed a BEM–FEM combined numerical model to investigate the wave–seabed–structure coupling interaction. In their model, Poisson's equations were used to govern the irrotational wave field for incompressible, inviscous fluid; and poro-elastic Biot's consolidation equations were used to govern the porous seabed and structures. However, Poisson's equations were incapable of describing the complex motion of viscous sea water and pore water, for example, the wave breaking. Additionally, the poro-elastic Biot's consolidation equations could only be applicable for the cases in which low frequency of loading and low permeability of soil were involved. Recently, Jeng et al. (2013) develop an advanced integrated model (PORO-WSSI 2D) for the problem of wave–seabed–structure interaction, in which the Volume-Averaged Reynolds Averaged Navier–Stokes (VARANS) equations are used to govern the wave motion and porous flow in seabed/breakwater, the dynamic Biot's equations (known as “ u - p ” approximation) are used to govern the behaviors of porous seabed and marine structures. The continuity of pressure and flux at the interface between seawater and the seabed/marine structures is applied in numerical computation. Due to that the VARANS equations are adopted in PORO-WSSI II, the complicated wave motion, for example, the wave breaking, can be simulated (Lin and Liu, 1998).

In view of the fact that a breaking wave is much more dangerous for the stability of breakwater than that of a non-breaking wave, the interaction between a breaking wave, seabed and breakwater increasingly attracts the attention from coastal engineers and academic researchers in recent years. Recently Ulker et al. (2012) numerically investigate the dynamics of a caisson breakwater under breaking wave loading. In their model, the wave impacts acting on the lateral side of caisson are determined according to the method proposed by Oumeraci et al. (2001), which is based on the probability theory in the frame of PROVERBS project; and the water pressure acting on the seabed surface is determined according to the Stokes linear wave theory. Obviously, this kind of method of applying the wave loading on caisson and seabed surface is illogical due to the fact that the wave breaking could not occur for a linear wave. This numerical model cannot describe the mechanism

of breaking wave–seabed–breakwater interaction. It led to the fact that the seabed foundation under the rubble mound could be liquefied in their analysis. Actually, it is impossible due to the fact that the upward seepage force beneath the rubble mound cannot overcome the weight of overburdened soil and caisson breakwater. In the practice of engineering, due to the lack of an effective analysis tool for coastal engineers for the wave–seabed–structures interaction problem, the empirical formulations based on experimental data are frequently adopted to estimate the wave impacts on vertical seawalls or caissons, and to evaluate the dynamics of breakwater in design. The reviews on the empirical formulations estimating the wave impact acting on breakwater, and the models determining the dynamics of breakwater under wave impact can be found in Cuomo et al. (2010), Cuomo et al. (2011b) and Cuomo et al. (2011a). Clearly, the interaction between breaking wave, seabed and breakwater is not sufficiently taken into consideration if the empirical formulations of wave impact are adopted in design.

In this study, we adopt the integrated model PORO-WSSI 2D developed by Ye (2012a) and Jeng et al. (2013) to investigate the interaction between breaking wave, seabed foundation and composite breakwater. Because the VARANS equations and the dynamic Biot's equations are coupled together in analysis, the mechanism of breaking wave–seabed–structures interaction could be revealed more realistically. Due to the fact that poro-elastic soil model is used for the seabed foundation soil in this study, the dynamics of seabed foundation is a transient response, rather than a residual response. It is noted that the compressive stress is taken as positive; and the displacement owning the same direction with x - z axes is taken as positive in PORO-WSSI 2D.

2. Integrated numerical model (PORO-WSSI 2D)

2.1. Wave model

The flow field inside and outside of porous media is governed by the VARANS (Volume-Averaged Reynolds Averaged Navier–Stokes) equations (Hsu et al., 2002). The mass and momentum conservation equations can be expressed as

$$\frac{\partial \langle \bar{u}_{fi} \rangle}{\partial x_i} = 0 \quad (1)$$

$$\frac{\partial \langle \bar{u}_{fi} \rangle}{\partial t} + \frac{\langle \bar{u}_{fi} \rangle}{n(1+c_A)} \frac{\partial \langle \bar{u}_{fi} \rangle}{\partial x_j} = \frac{1}{1+c_A} \left[-\frac{n}{\rho_f} \frac{\partial \langle \bar{p} \rangle}{\partial x_i} - \frac{\partial \langle \bar{u}_{fj} \bar{u}_{fi} \rangle}{\partial x_j} + \frac{1}{\rho_f} \frac{\partial \langle \bar{\tau}_{ij} \rangle}{\partial x_j} + ng_i \right] - \frac{\langle \bar{u}_i \rangle}{1+c_A} \left[\frac{\alpha(1-n)^2}{n^2 d_{50}^2} + \frac{\beta(1-n)}{n^2 d_{50}} \sqrt{\langle \bar{u}_{f1} \rangle^2 + \langle \bar{u}_{f2} \rangle^2} \right] \quad (2)$$

where u_{fi} is the flow velocity, x_i is the Cartesian coordinate, t is the time, ρ_f is the water density, p is the pressure, τ_{ij} is the viscous stress tensor of mean flow, g_i is the acceleration due to gravity, and n and d_{50} are the porosity and the equivalent mean diameter of the porous material. c_A denotes the added mass coefficient, calculated by $c_A = 0.34(1-n)/n$. α and β are empirical coefficients associated with the linear and nonlinear drag force, respectively. Through the fitting and regression of a wide range of experiment data, Liu et al. (1999) suggested that the $\alpha = 200$ and $\beta = 1.1$ for porous flow. Recently, Lara et al. (2011) recommend two nonlinear relations relating the empirical coefficients α and β to the porosity n and mean particle size d_{50} : $\alpha = 4409.22d_{50}$, $\beta = 12.27 \frac{n^2}{(1-n)^{1.5}} d_{50}^{-0.1075}$, “ $\langle \cdot \rangle$ ” and “ $\langle \cdot \rangle^f$ ” stand for Darcy's volume averaging operator and the intrinsic averaging operator, respectively.

In the VARANS equations, the interfacial force between pore fluid and solid matrix is modeled according to the extended Forchheimer relationship, in which both linear and nonlinear drag forces between the pore water and the skeleton of porous structures, and the inertia added mass are included in the last term of Eq. (2). The influence of

turbulence fluctuations on the mean flow ($\langle \bar{u}_{fi} \rangle$), denoted as $\langle u'_{fi} u'_{fi} \rangle$, is obtained by solving the volume-averaged $k - \epsilon$ turbulence model.

The above VARANS equations for flow field outside and inside of porous medium are solved by using the finite difference two-step projection method on a staggered grid system for space discretization, and the forward time difference method for time derivative. The VOF method is applied to track water free-surface. The combined central different method and upwind method are used to solve the $k - \epsilon$ equations. In this wave model, the internal wave maker proposed by Lin and Liu (1999) is applied to generate the target wave train, in which a mass function is added to the continuity in Eq. (1).

2.2. Soil model

The dynamic Biot's equation known as “ $u-p$ ” approximation proposed by Zienkiewicz et al. (1980) is used to govern the dynamic response of the porous medium under wave loading, in which the relative displacements of pore fluid to soil particles are ignored, but the acceleration of pore water and soil particles are included:

$$\frac{\partial \sigma'_x}{\partial x} + \frac{\partial \tau_{xz}}{\partial z} = -\frac{\partial p}{\partial x} + \rho \frac{\partial^2 u}{\partial t^2}, \quad (3)$$

$$\frac{\partial \tau_{xz}}{\partial x} + \frac{\partial \sigma'_z}{\partial z} + \rho g = -\frac{\partial p}{\partial z} + \rho \frac{\partial^2 v}{\partial t^2}, \quad (4)$$

$$k \nabla^2 p - \gamma_w n \beta \frac{\partial p}{\partial t} + k \rho_f \frac{\partial^2 \epsilon_v}{\partial t^2} = \gamma_w \frac{\partial \epsilon_v}{\partial t}, \quad (5)$$

where (u, v) = the soil displacements in the horizontal and vertical directions, respectively; n = soil porosity; σ'_x and σ'_z = effective normal stresses in the horizontal and vertical directions, respectively; τ_{xz} = shear stress; p = the pore water pressure; $\rho = \rho_f n + \rho_s (1 - n)$ is the average density of porous seabed; ρ_f = the fluid density; ρ_s = solid density; k = the Darcy's permeability; g = the gravitational acceleration, γ_w is unit weight and ϵ_v is the volumetric strain. In Eq. (5), the equivalent compressibility of pore water and entrapped air (β) and the volume strain (ϵ_v) are defined as

$$\beta = \left(\frac{1}{K_f} + \frac{1 - S_r}{p_{w0}} \right), \quad \text{and} \quad \epsilon_v = \frac{\partial u}{\partial x} + \frac{\partial v}{\partial z}, \quad (6)$$

where S_r = the degree of saturation of seabed, p_{w0} = the absolute static pressure and K_f = the bulk modulus of pore water.

The finite element method is used to solve the above governing Eqs. (3) to (5). The discretized governing equations are

$$\mathbf{M}\ddot{\mathbf{u}} + \mathbf{K}\mathbf{u} - \mathbf{Q}\dot{\mathbf{p}} = \mathbf{f}^{(1)} \quad (7)$$

$$\mathbf{G}\ddot{\mathbf{u}} + \mathbf{Q}^T \dot{\mathbf{u}} + \mathbf{S}\dot{\mathbf{p}} + \mathbf{H}\mathbf{p} = \mathbf{f}^{(2)} \quad (8)$$

The generalized Newmark p^{th} order scheme for j^{th} order equation scheme is adopted to calculate time integration when solving the above discretized matrix equations. The definition of coefficient matrixes \mathbf{M} , \mathbf{K} , \mathbf{Q} , \mathbf{G} , \mathbf{S} , \mathbf{H} , $\mathbf{f}^{(1)}$, $\mathbf{f}^{(2)}$, and the detailed information for the numerical method to solve the dynamic Biot's equation can be found in (Ye, 2012a).

In PORO-WSSI 2D, the above wave model and soil model are integrated/coupled together through a developed one way coupling algorithm. This one way coupling algorithm can guarantee the continuous water pressure and flow velocity on the interface between fluid domain and solid domain. However, the displacement is not continuous on the same interface. Due to the fact that the wave-induced displacement of

marine structures and seabed floor is generally apparently small comparing with wavelength, the discontinuity of displacement on their interface is acceptable. More detailed information about the integration method can be found in Ye (2012a) and Jeng et al. (2013).

The validity and reliability of the developed and integrated/coupled numerical model PORO-WSSI 2D have been widely verified by Ye (2012a) and Jeng et al. (2013). The good agreement between the numerical results predicted by PORO-WSSI 2D and the experimental data indicates that PORO-WSSI 2D is highly reliable for the problem of wave-elastic seabed-structure interaction. Actually, the authors also try to find a wave flume test involving wave breaking in front of a breakwater available in previous literature to further verify PORO-WSSI 2D; however, it is found that there is no a suitable wave flume test that could achieve this goal, including the experimental tests conducted by Cuomo et al. (2010); because there is no porous sand bed foundation under breakwater when the wave breaks in front of the breakwater. The only way to validate PORO-WSSI 2D on the problem of breaking wave-seabed-breakwater interaction, is to conduct the wave flume test by ourselves in the future.

3. Analysis of breaking wave-seabed foundation-breakwater interaction

The integrated model PORO-WSSI II is adopted to investigate the interaction between a breaking wave, composite breakwater and its seabed foundation. We focus our attention on the dynamic response of seabed and composite breakwater, and the liquefaction in seabed foundation under breaking wave loading. The configuration of computational domain is shown in Fig. 1. In the configuration, a composite breakwater is built on the sloping seabed floor (gradient: 2:100). The caisson is treated as a rigid and impermeable block in computation. The seabed and rubble mound are considered as two different types of porous medium. The properties of seabed soil, rubble mound, and the wave characteristics propagating on the seabed floor are listed in Table 1.

Due to the fact that the caisson is treated as an impermeable block constructed on the rubble mound, there is an upward buoyancy acting on the bottom of the caisson. In most previous studies, this buoyancy was neglected (Jeng et al., 2000, 2001; Ulker et al., 2010). Obviously, the initial effective stresses in the seabed foundation beneath the composite breakwater could be overestimated if the upward buoyancy was neglected in computation (Ye, 2012b; Ye et al., 2012). It would further lead to underestimate the maximum liquefaction depth in the seabed foundation under wave loading. In this study, the upward buoyancy acting on the bottom of caisson is taken into consideration when determining the initial consolidation state, and predicting the maximum liquefaction depth in the seabed foundation.

The following boundary conditions for this computational domain are applied in computation:

- (1) The bottom of seabed foundation is treated as rigid and impermeable:

$$u = v = 0 \quad \text{and} \quad \frac{\partial p}{\partial z} = 0 \quad \text{at} \quad z = 0. \quad (9)$$

- (2) The two lateral sides of seabed are fixed in x direction:

$$u = 0 \quad \text{at} \quad x = 650\text{m} \quad \text{and} \quad x = -300\text{m}. \quad (10)$$

- (3) The surface of seabed, and the outer surface of rubble mound, concrete caisson are applied perpendicularly by hydrostatic pressure, and wave-induced dynamic pressure. The pore pressure is continuous at the interface between the seabed, breakwater and the sea water.

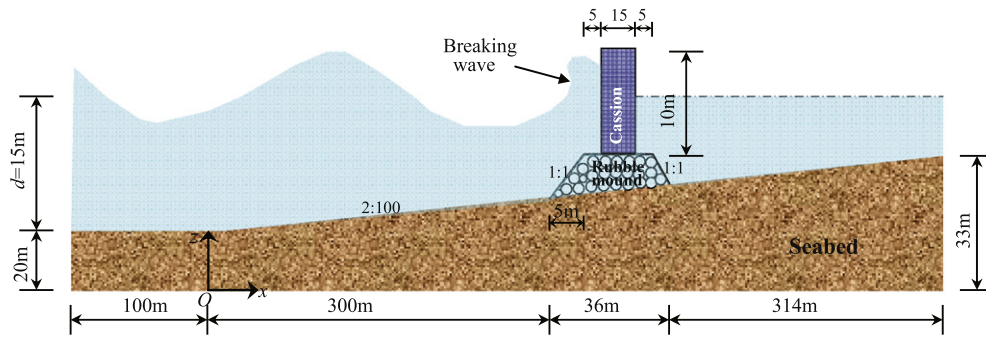


Fig. 1. Configuration of computational domain for the problem of breaking wave–seabed–breakwater interaction.

- (4) There is an upward floating force acting on the bottom of concrete caisson due to its impermeability.

In the fluid domain, orthogonal grid is used. The mesh size in x direction is 0.35–0.5 m; it is 0.1–0.2 m in z direction. In the solid domain, the FEM mesh in x direction is 2.0–4.0 m; it is 0.12–1.3 m in z direction. Dense mesh is used in the zone around the composite breakwater both in fluid and solid domains. Additionally, the FEM mesh in the surface zone of seabed floor is much denser than that in the lower seabed floor. In total, 15000 8-node isoparametric elements are used in solid domain. The wave length L is about 100 m. The ratio between the characteristic wave length and the maximum mesh size is 200 in fluid domain; and it is 50 in the zone around the composite breakwater in the solid domain. The convergence analysis in Ye et al. (in press) indicates that this mesh system can make the results be convergent. The numerical wave maker in fluid domain is located at $x = -200$ m, which is 600 m away from the composite breakwater. This long distance could make the wave be mature before interacting with the breakwater.

In the practice of engineering, some heavy concrete blocks are generally placed on the rubble mound to protect the composite breakwater. However, these heavy concrete blocks on the rubble mound are not included in computation due to the following three aspect challenge. (1) The interface between these concrete blocks and seawater is so complex that it could not be dealt with by the present numerical model PORO-WSSI 2D. (2) The porous flow in these concrete blocks armor is generally highly turbulent with high Reynolds number; however, the Biot's equation is not applicable to turbulent porous flow. (3) The empirical coefficients α and β in the VARANS equation would be difficult to be determined accurately. In order to simplify the problem of breaking wave–seabed–structure interaction, the concrete block armor is not included as that in Ulker et al. (2010), Ulker et al. (2012) and Jeng et al. (2001) etc.

3.1. Breaking wave-induced impact on caisson

Due to the fact that the ocean wave generated by the wave maker propagates on a sloping seabed floor, the water depth decreases gradually. The potential for the wave to break increases gradually. When the wave propagates to the caisson, it collides with the caisson, and then

Table 1
Properties of seabed soil, rubble mound and the wave characteristics.

Medium	H (m)	d (m)	t (s)	G (N/m ²)	ν	k m/s	n	d_{50} (mm)	Sr
Wave	4.0	15.0	10.0						
Seabed				6.0×10^7	0.333	1.0×10^{-4}	0.25	0.02	0.98
Rubble mound				1.0×10^8	0.333	2.0×10^{-1}	0.35	500	0.99
Caisson				5.0×10^{10}	0.25	0.0	0.0	-	0.0

reflects. The wave finally breaks in front of the caisson. In the process of colliding, reflecting and breaking, the wave will apply a great push force on the lateral side of the caisson. Investigation of this force acting on the lateral side of caisson quantitatively is very important for coastal engineers involved in the design of composite breakwaters. Some previous literatures adopted the probability theory or empirical formulations to estimate the magnitude of impact acting on caisson and the rising time of the maximum impact (Oumeraci et al., 2001; Walkden et al., 1996). More detailed information about the determination of the impact acting on vertical structures using probability theory or empirical formulations can be found in Cuomo et al. (2011b). Undoubtedly, the probability theory and empirical formulations cannot accurately describe the time history curve of the breaking wave-induced impact acting on the caisson. And the results determined by probability theories or empirical formulations are only approximation. In this study, the breaking wave-induced impact acting on the caisson can be determined due to the fact that the wave model in PORO-WSSI 2D would effectively simulate the interaction between the sea water and the caisson breakwater. Fig. 2 illustrates the time history curve of impact acting on the lateral side of the caisson in three typical time periods. As illustrated in Fig. 2, the breaking wave-induced impact acting on the caisson increases to its maximum value, and decreases to its minimum value in a short time. Therefore, the impact effect of the force on the caisson will be very significant. It is further found that the most obvious characteristic of the breaking wave-induced impact on the caisson is that there is a vibration when the impact reaches its peak area, making an 'M' shape in each peak area. The non-breaking wave-induced force on the caisson has no this phenomenon. It is indicated that this vibration of impact on caisson in each peak area is related to the wave breaking when each crest of wave arrives at the composite breakwater. Fig. 3 shows the whole time history curve of the wave-induced force acting on the lateral side of the caisson.

Fig. 4 demonstrates the vertical distribution of the breaking wave-induced dynamic pressure acting on the caisson at different times from $t = 80$ s to 90 s. In Fig. 4, it is found that the upper part of the caisson is applied by the breaking wave when it runs up in front of the caisson; and most of the lower part of the caisson is free when the breaking wave runs down. From the analysis above, it is shown that the integrated model PORO-WSSI 2D is capable of determining the breaking wave-induced impact acting on the caisson quantitatively and accurately. This is very important when investigating problem of the wave, seabed and composite breakwater interaction.

It is worthy to note that the air over the seawater is not considered in the wave model when determining the impact on the breakwater induced by the breaking wave. From the point of view of physics, some air would be entrapped by seawater when the wave breaks in front of the breakwater; and the mixture of seawater–air is formed. If the entrapped air is not considered in the numerical wave model, the wave breaking-induced void in seawater is vacuous. The compressibility of seawater–vacuous void is significantly much greater than that of seawater–entrapped air mixture. As a result, breaking

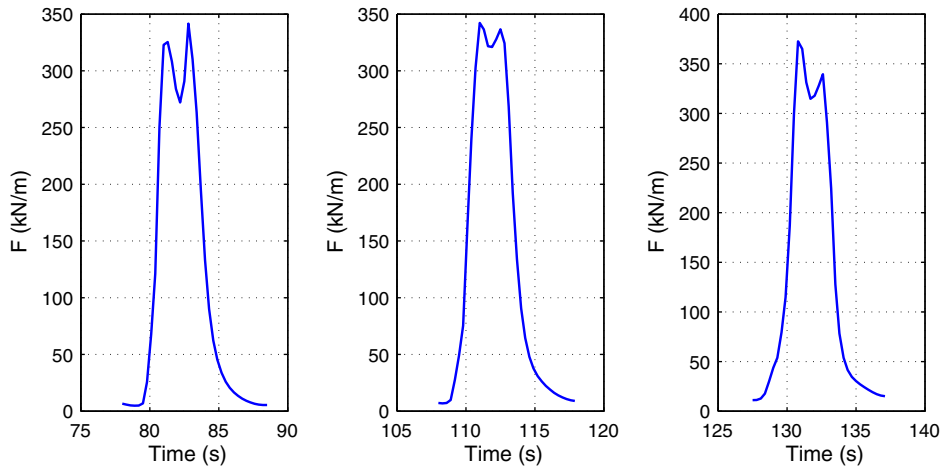


Fig. 2. Breaking wave-induced impact on the lateral side of the caisson in three typical time periods.

wave-induced impact on breakwater predicted by the numerical wave model is generally less than the actual impact.

This phenomenon is also observed by Hsiao and Lin (2010). In their work, The RANS equation (COBRAS) was used to simulate a solitary wave impinging and overtopping an impermeable seawall. The comparison for the wave-induced impact on the leeward side seawall, where wave overtopping and breaking occurs, indicates that the peak values of impact predicted by numerical model (in which air is not considered) are less than the measured ones. However, the difference between the numerical and measured results is not large.

Consideration of the existence of entrapped air in breaking wave is an interesting and researchable topic in the future. The effect of the seawater–entrapped air mixture in breaking wave on the impact acting on marine structures, and the magnitude of difference between numerical results and actual measured impact if the air phase is ignored in numerical model, need further investigation.

3.2. Consolidation of seabed under composite breakwater

In the offshore environment, seabed generally has experienced the consolidation process under the seawater loading and self-gravity in the geological history. Additionally, after composite breakwater is constructed on seabed, the seabed beneath and near to the composite breakwater will be compressed, and deformed under the gravity of composite breakwater. Finally, the seabed will reach a new balanced state based on the previous consolidation status under hydrostatic sea

water pressure and composite breakwater loading. From the point of view of physics, in order to simulate the interaction between ocean wave, seabed and marine structures, the initial consolidation state of seabed foundation under hydrostatic pressure and the gravity of composite breakwater should be determined first. Then, this consolidation status is taken as the initial condition for the wave–seabed–structure interaction problem.

Fig. 5 illustrates the distributions of the effective stresses, the shear stress and the pore pressure in the porous seabed under hydrostatic pressure and the gravity of composite breakwater after the seabed foundation consolidates adequately. Fig. 6 shows the distributions of the horizontal and vertical displacements in the seabed foundation. It can be seen in Fig. 5 that the contours of pore pressure in seabed foundation are basically layered, which is consistent with the distribution of hydrostatic water pressure. The magnitudes of the effective stresses in the seabed foundation under the composite breakwater increase significantly comparing with that when there are no marine structures. Additionally, there are two zones in the seabed near to the two feet of the rubble mound where the shear stress concentrates. It is possible for this concentrated shear stress to make the seabed foundation fail (known as shear failure) in the practice of engineering. Fig. 6 indicates that the composite breakwater subsides about 30 mm induced by its gravity; and the seabed foundation is compressed, and the soil particles move toward two sides. Due to the fact that the composite breakwater is built on the coastal slope (sloping seabed floor near to the coastal line), the horizontal displacement at the two sides of the composite

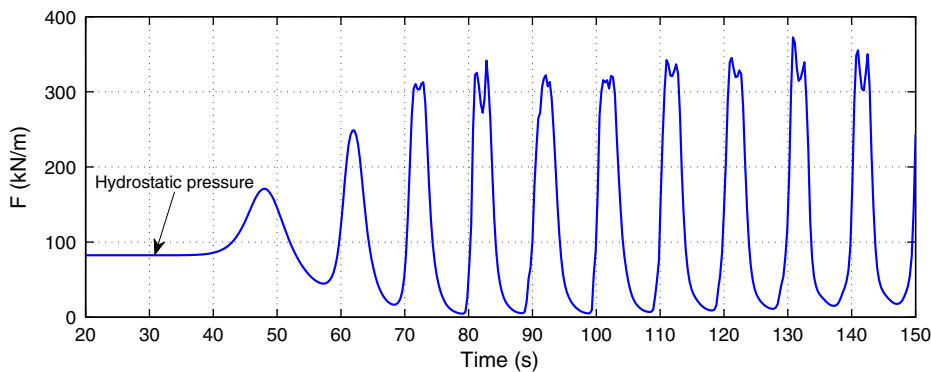


Fig. 3. Time history curve of impact force acting on the lateral side of the caisson (note: the hydrostatic pressure is included).

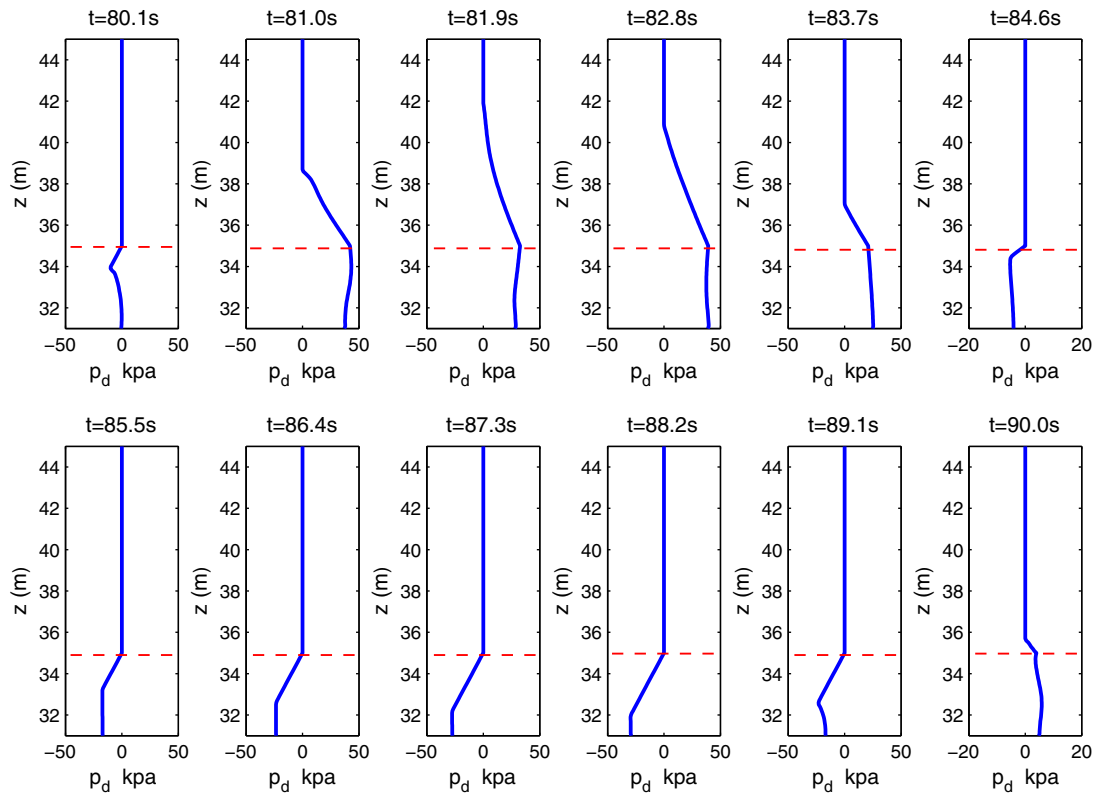


Fig. 4. Distribution of the breaking wave-induced dynamic pressure acting on the caisson at different times. Red dotted line is the elevation of static water level.

breakwater is asymmetric. The horizontal displacement at the left hand side of the composite breakwater is obviously greater than that at the right hand side.

3.3. Breaking wave-induced dynamic response of caisson and seabed

Ocean waves with large height (carrying huge energy) propagate along coastal slope from deep sea to breakwater, and collide with breakwater. In the process of collision, the large waves break; meanwhile the breakwaters are attacked dangerously by the breaking wave. This interaction between the large wave and the breakwater makes the breakwater much easier to fail. The failure generally includes two types. The first one is that the caisson is overthrown by the crest of breaking wave; the second type is that the seabed foundation beneath the breakwater is liquefied when the trough of wave arrives at the breakwater. Therefore, it is important to predict the dynamic response of caisson and seabed foundation under breaking wave loading.

By adopting the integrated model PORO-WSSI II, we first simulate a regular ocean wave propagating on the coastal slope, and interacting with the composite breakwater using the wave model. The pressure (hydrostatic and dynamic pressures) acting on seabed and on the composite breakwater is correspondingly determined. Taking the original consolidation state determined above as the initial condition, the soil model is used to predict the response of the seabed foundation and the composite breakwater under the breaking wave loading. Two typical times ($t = 82.0$ s and $t = 87.0$ s) are chosen to demonstrate the breaking wave-induced dynamic response of the caisson and the seabed. At time $t = 82.2$ s, a crest of wave arrives at the caisson, and breaks. At time $t = 87.0$ s, a wave trough arrives at the caisson.

Undoubtedly, the caisson will vibrate periodically under the application of the wave. This wave-induced vibration of the caisson is one of the key problems for coastal engineers involved in the design of a marine structure. The excessive vibration magnitude would make the caisson easier to generate the fatigue failure. Controlling the vibration

magnitude of caisson is necessary in the practice of engineering. Fig. 7 shows the horizontal and vertical displacements of the right vertex of the caisson under the breaking wave loading.

In Fig. 7, it can be found that the wave does not break at the beginning stage when the wave arrives at the caisson. Due to the blocking effect of the breakwater, the wave reflects, and interferes with the incident wave; the wave height increases gradually. When the third crest arrives at the caisson, the wave begins to break, and attack the breakwater. From then on, once the wave crest arrives at the caisson, and breaks; the caisson sways in a short period on both horizontal and vertical directions. This results in a series of 'M' shape zone on the history time curves of the wave-induced dynamic horizontal and vertical displacements.

The wave-induced pore pressure in the rubble mound and in the seabed foundation is a key factor to affect the transient liquefaction potential of seabed. It is interesting to study how the breaking wave affects the pore pressure in the rubble mound and seabed foundation. Here, three typical points, A ($x = 218.5$ m, $z = 28.685$ m in the rubble mound), B ($x = 200$ m, $z = 26.0$ m on the seabed) and C ($x = 218.5$ m, $z = 23.9358$ m in the seabed) are chosen. Fig. 8 illustrates the variation of the breaking wave-induced pore pressure at points A, B and C. In Fig. 8, it is found that the effect of the breaking wave on the pore pressure in the rubble mound and seabed foundation is significant at point A (in the rubble mound) and B (on the seabed). When the crest of wave arrives at the caisson, and then breaks, the pressure acting on the seabed and on the composite breakwater, and the pore pressure in the rubble mound also vibrate in a short period like that of the displacements of caisson under the breaking wave loading. However, the vibration magnitude of the pore pressure at Point A (in rubble mound) is much smaller than that at point B (on the seabed). It is indicated that the rubble mound has blocking effect on the breaking wave to some extent. There is no vibration on the history time curve of the pore pressure at point C (in the seabed). It further indicates that the effect of breaking wave on the pore pressure in the seabed mainly concentrates

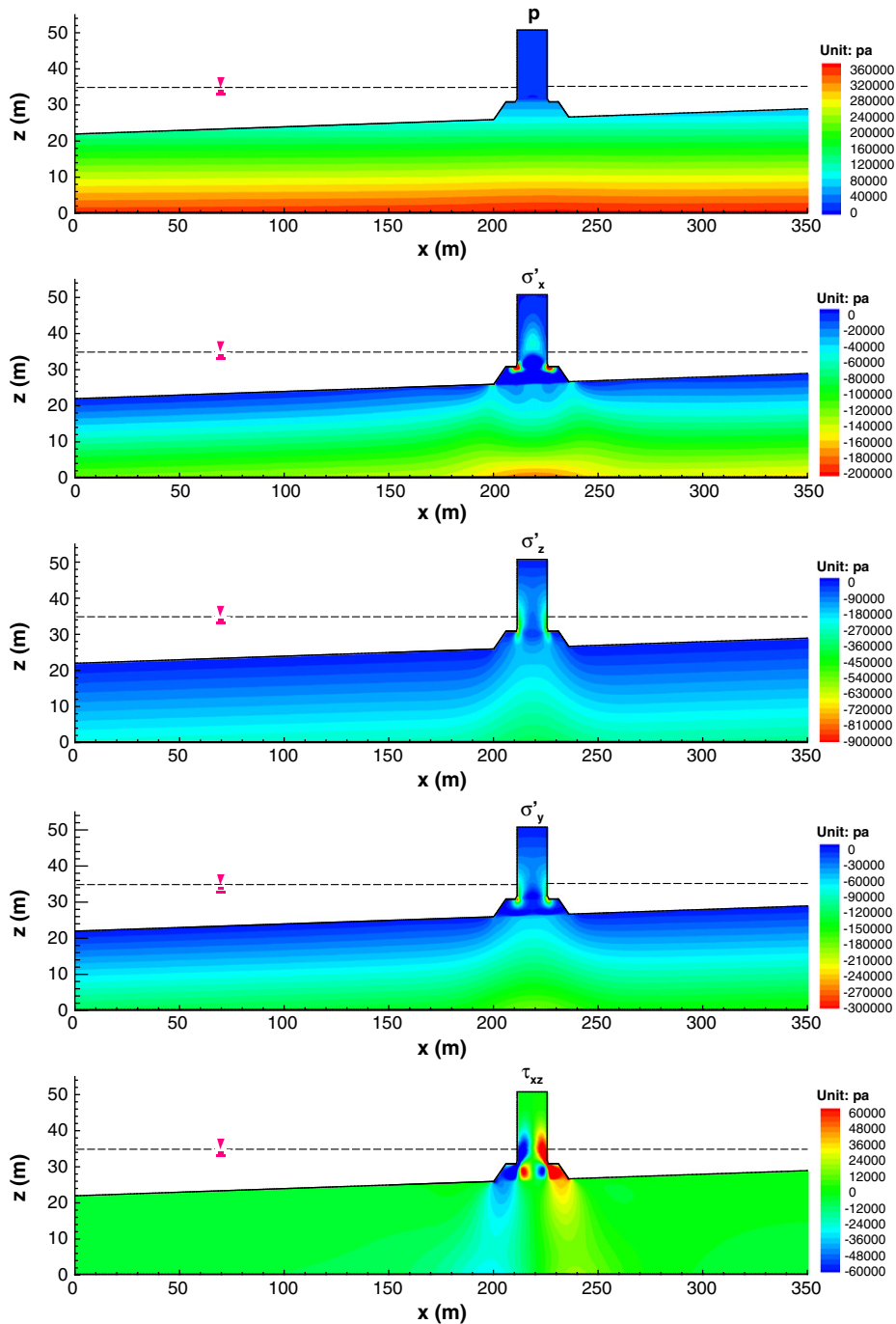


Fig. 5. Distribution of pore pressure, effective stresses in the seabed foundation and composite breakwater in the consolidation status.

in the zone near to the seabed surface. The effect gradually disappears due to the blocking effect of the rubble mound and upper seabed foundation.

As we know, Biot's dynamic equation was established based on the Darcy's laminar flow. For the nonlinear and turbulent porous flow, it is not applicable. Some previous investigation pointed out that Biot's dynamic equation is applicable when Reynolds number is less than 10 ($Re \leq 10$). However, the analysis conducted by Ye (2012a) and Jeng et al. (2013) for the porous flow in a large-scale rubble mound indicates that this conclusion would be controversial. The wave-induced dynamic pressure in the rubble mound determined by Biot's dynamic equation and VARANS equation, respectively, is basically the same even the Reynolds number ($Re = \sqrt{u^2 + v^2} \times d_{50} / \nu$) reaches up to 8000. This

result indicates that the application range of Biot's dynamic equation would be much larger than we expected, because the Reynolds number of porous flow is not only dependent on the flow speed, but also dependent on the mean particle size d_{50} . For the porous flow in rubble mound, the speed maybe is small; however, the mean particle size d_{50} is relatively huge. As a result, the Reynolds number in rubble mound seems very great. Under this situation, the Biot's dynamic equation would be still applicable, because the flow speed of pore water is small. In the authors' opinion, the application range of Reynolds number for classic Biot's dynamic equation needs further investigation in the future.

At time $t = 82.2$ s, the fourth crest of the wave arrives at the caisson, and breaks. At this time, the breaking wave attacks the caisson with a

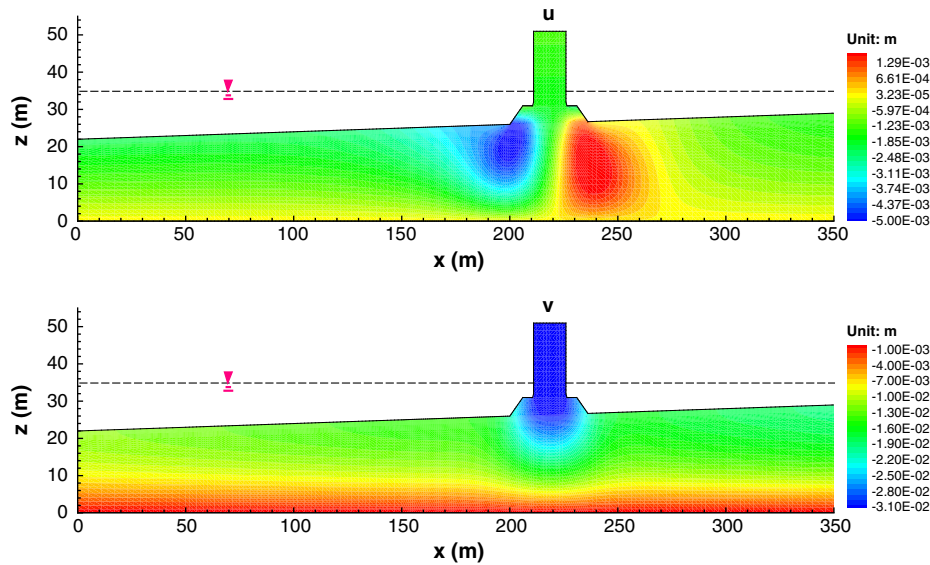


Fig. 6. Distributions of displacements in the seabed foundation and composite breakwater in the consolidation status.

large impact. It is quite possible for the composite breakwater to generate fatigue failure if the wave applies its loading for a long time. At time $t = 87.0$ s, the fourth wave trough arrives at the caisson. At this time, the seabed foundation is quite possible to liquefy. Therefore, it is meaningful to investigate the wave field and dynamic response of the composite breakwater and the seabed foundation at the two typical times.

Fig. 9 shows the free surface and the velocity field at time $t = 82.2$ s and $t = 87.0$ s. It can be seen that the wave breaks at time $t = 82.2$ s when interacting with the caisson. The velocity field in the zone near to the caisson is affected greatly by the breaking wave both at times $t = 82.2$ s and $t = 87.0$ s. As a supporting evidence, Fig. 10 illustrates the distribution of the turbulent energy k at the two typical times.

Fig. 10 explicitly indicates that the wave breaks when it collides with the caisson.

Figs. 11 and 12 demonstrate the distribution of the breaking wave induced dynamic pore pressure, effective stresses and shear stress in the seabed foundation at times $t = 82.2$ s and $t = 87.0$ s.

From Figs. 11 and 12, it is obviously found that the wave-induced dynamic pore pressure in seabed mainly concentrates in the zone near to the seabed surface. This is the reason why the wave-induced liquefaction in seabed always occurs in the upper seabed. It also can be seen that the vertical effective stress σ'_z , the horizontal effective stresses σ'_x and σ'_y are all compressive (compression taken as negative) under wave crest; while they are all tensile under wave trough. An interesting phenomenon found from the distributions of wave induced

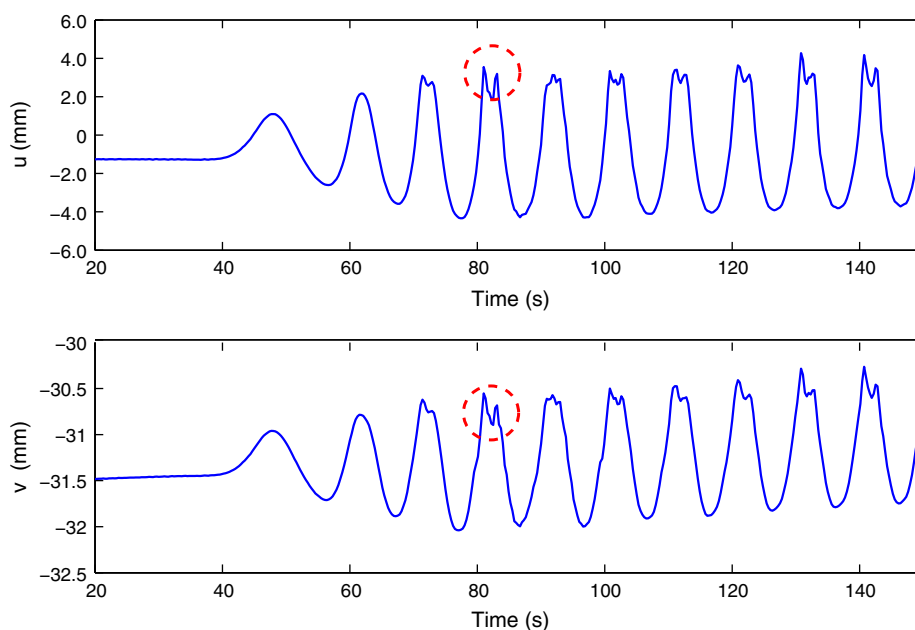


Fig. 7. History time curve of the horizontal and vertical displacements of the right vertex of caisson under the breaking wave loading.

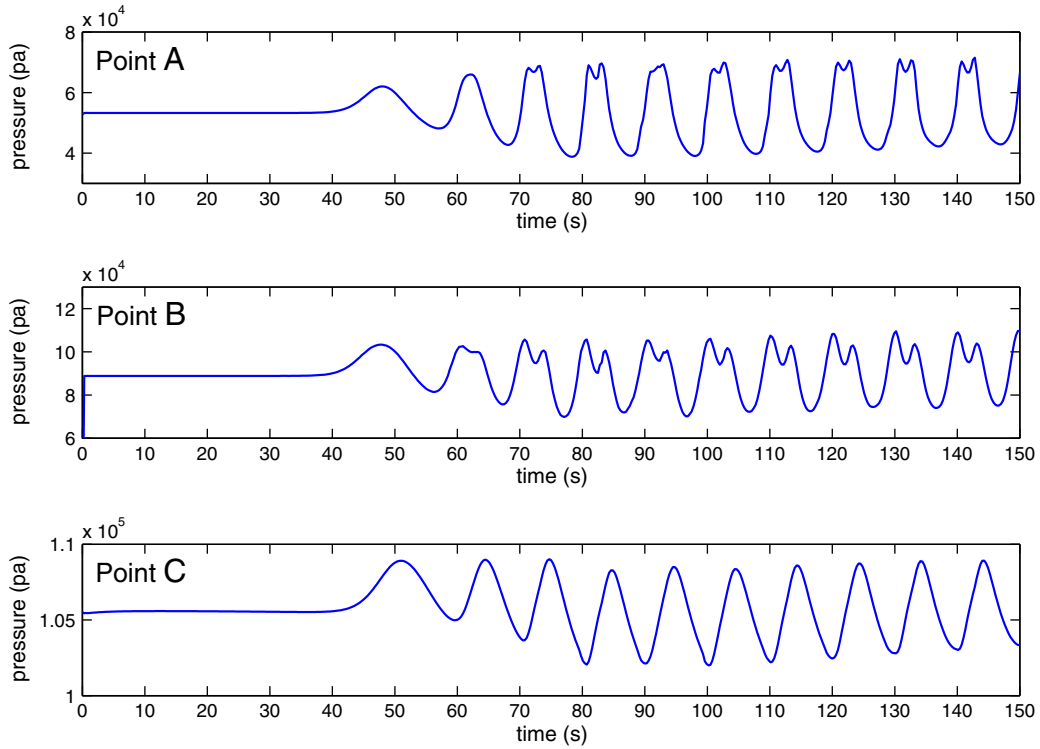


Fig. 8. Variation of the breaking wave induced pore pressure on typical points A ($x = 218.5$ m, $z = 28.685$ m), B ($x = 200$ m, $z = 26.0$ m) and C ($x = 218.5$ m, $z = 23.9358$ m).

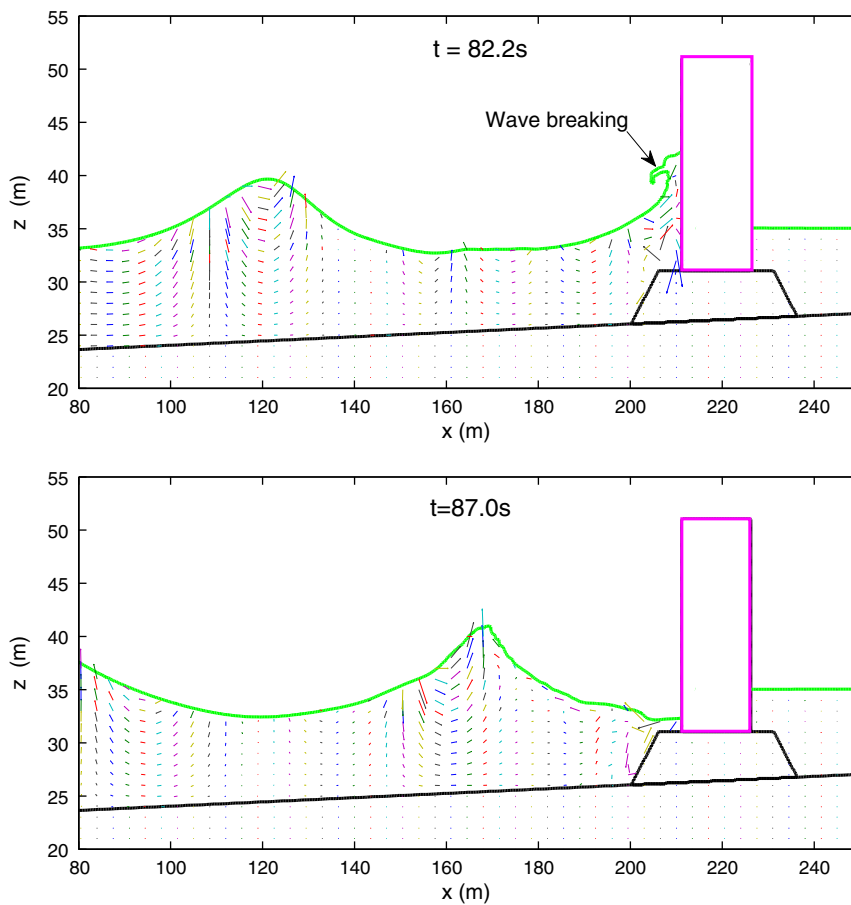


Fig. 9. Free surface and velocity field at two typical times $t = 82.2$ s and $t = 87.0$ s in fluid domain.

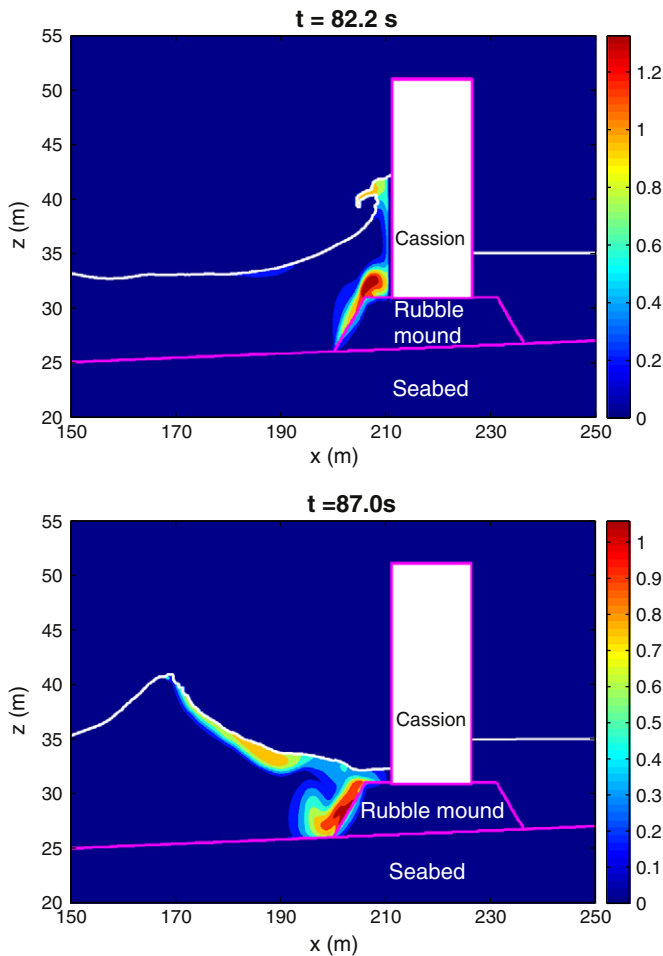


Fig. 10. Distribution of turbulent energy k at two typical times $t = 82.2$ s and $t = 87.0$ s in fluid domain.

shear stress τ_{xz} in the seabed foundation at the two typical times is that there is about $\pi/4$ phase lag between the wave-induced shear stress in the seabed and the wave propagating on the seabed.

3.4. Liquefaction in seabed foundation

It has been commonly recognized that the seabed would liquefy under wave loading. This kind of liquefaction in seabed could attribute to the wave induced dynamic pressure acting on seabed when the ocean wave propagates on it. The wave-induced dynamic pressure makes the effective stresses in seabed vary accordingly. The effective stresses and pore pressure in seabed decrease based on its initial consolidation state when the wave trough propagates on it. When the effective stresses at some regions in seabed decrease to zero, the soil in the region liquefies immediately. As we know, the liquefied seabed behaves like a kind of heavy liquid. There is no any bearing capacity to support structures. Therefore, the liquefied seabed is a fatal factor for the marine structures constructed on it. The liquefaction potential of seabed beneath and closed to a marine structure, such as composite breakwater, is an important issue for coastal engineers when designing and maintaining marine structures. The assessment and prediction of the liquefaction potential of seabed under breaking wave loading in the offshore environment are significantly necessary in the practice of engineering.

The seabed is a kind of porous medium, consisting of soil particles, pore water and air. The soil particles form the skeleton, and the pore water and air occupy the void between the soil particles. When an ocean wave propagates on the seabed, the seabed is applied with the

wave-induced dynamic pressure. The pore water is driven by the dynamic pressure to flow in and out of the seabed. Meanwhile, the seepage force in seabed acting on the soil particles applied by the flowing pore water is formed. The seepage force in seabed is dependent on the gradient of pore pressure in seabed, defined as

$$j_x = \frac{\partial p}{\partial x} \quad \text{and} \quad j_z = \frac{\partial p}{\partial z} \quad (11)$$

$$j = \sqrt{j_x^2 + j_z^2} \quad (12)$$

Fig. 13 shows the distribution and vectors of the seepage force in the region near to seabed surface at times $t = 82.2$ s and $t = 87.0$ s. In Fig. 13, it is found that the vertical component of the seepage force is much greater than the horizontal component; and the seepage force is upward under wave trough; while it is downward under wave crest. Generally, the liquefaction potential is directly related to the magnitude and direction of the seepage force. The seabed is likely to liquefy when the seepage force is upward because it will decrease the contact effective stresses between soil particles. However, the seabed will absolutely not liquefy when the seepage force is downward under wave crest because it will increase the contact effective stresses of soil particles. Another obvious phenomenon observed from Fig. 14 is that the wave driven seepage force in seabed is mainly distributed in the zone near to the seabed surface. In other zones, the wave driven seepage force is not significant. It is indicated that the effect of wave on the liquefaction of seabed in the zone far away the seabed surface is limited.

In this study, in order to investigate the liquefaction properties in seabed under the breaking wave loading, the liquefaction criteria proposed by Okusa (1985) are used. It is expressed as:

$$(\gamma_s - \gamma_w)(h - z) \leq \sigma'_z \quad (13)$$

where the γ_s is the saturation unit weight of seabed soil, γ_w is the unit weight of water, h is the seabed thickness, in this case, it is a variable value dependent on the x coordinate and slope angle of seabed surface, and σ'_z is the wave-induced vertical dynamic effective stress. Actually, the liquefaction criteria (Eq. (13)) means that the seabed will liquefy if the wave-induced vertical dynamic effective stress σ'_z (note: compressive stress is negative) is equal to or greater than the original vertical effective stress $(\gamma_s - \gamma_w)(h - z)$. However, Eq. (13) is only applicable for the cases in which there is no marine structure constructed on the seabed, because the original vertical effective stress σ'_z in seabed could not be determined using the formula $(\gamma_s - \gamma_w)(h - z)$ in the region beneath and closed to the marine structures. The liquefaction criteria (Eq. (13)) have to be modified for the cases in which marine structures are constructed on seabed:

$$-(\sigma'_z)_{initial} \leq \sigma'_z \quad (14)$$

where $(\sigma'_z)_{initial}$ is the vertical effective stress in the initial consolidation state.

Fig. 14 shows the liquefaction zones in the seabed under the breaking wave loading at time $t = 82.2$ s and $t = 87.0$ s, in which the modified liquefaction criteria (Eq. (14)) are applied. As illustrated in Fig. 14, there are two liquefaction zones in the region near the seabed surface at time $t = 82.2$ s; they are located at the range of $x = 50$ m to $x = 100$ m, and $x = 150$ m to $x = 200$ m respectively. However, there is only one liquefaction zone in the region near to the seabed surface at time $t = 87.0$ s, which is located at the range of $x = 100$ m to $x = 150$ m. Comparing the liquefaction zones in Fig. 14, the position of wave trough and the upward seepage in Fig. 13, it is found that the seabed under wave trough indeed has liquefied (upward seepage); while the seabed under wave crest has no potential for liquefaction (downward seepage). However, it is interesting to observe that the

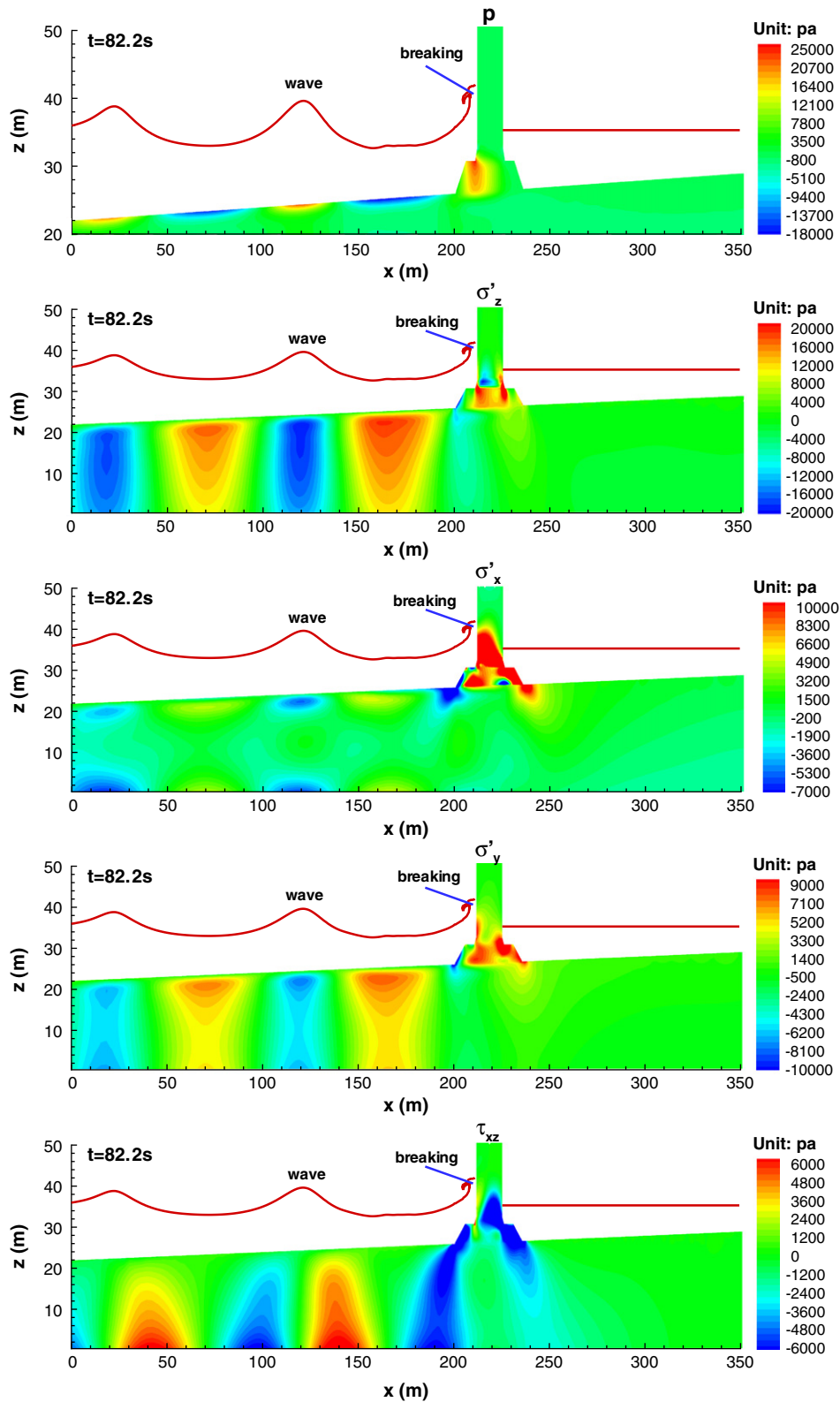


Fig. 11. Distribution of the breaking wave-induced dynamic pore pressure, effective stresses and shear stress in the seabed foundation at time $t = 82.2$ s.

seabed under the rubble mound does not liquefy at time $t = 87.0$ s even though the seepage force is upward and the trough of breaking wave is being on that part of the seabed. The reason is that the seabed under the rubble mound is compressed by the gravity of the composite breakwater. This compression induced by the gravity of the composite breakwater would effectively protect the seabed foundation from the

wave-induced liquefaction. Therefore, it is suggested that the rubble mounds with wider shoulder are recommended to use in practical engineering.

Due to the fact that the liquefaction zone ($x = 150$ m to $x = 200$ m) near to the composite breakwater is a potential dangerous factor to the stability of the composite breakwater under breaking wave loading, we

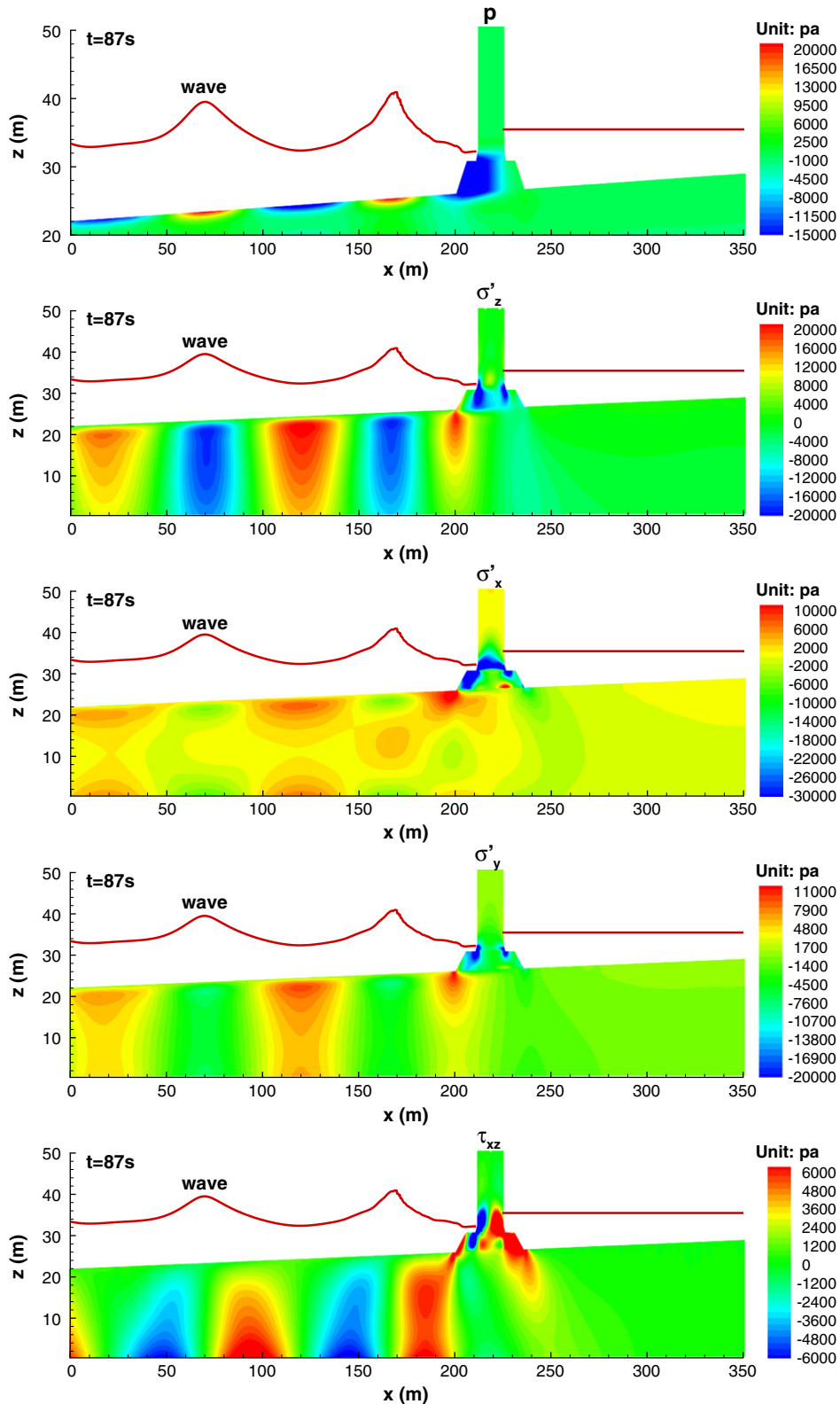


Fig. 12. Distribution of the breaking wave-induced dynamic pore pressure, effective stresses and shear stress in the seabed foundation at time $t = 87.0$ s.

emphasize our attention to study the liquefied depth of this liquefaction zone ($x = 150$ m to $x = 200$ m) in the following part.

Fig. 15 illustrates the liquefied depth on the line $x = 180.0$ m which is in the range of the liquefaction zone investigated. It is found that the soil on the line $x = 180.0$ m is not liquefied until $t = 70.0$ s, even though there is wave crest/trough passing through on it. After $t =$

70.0 s, the soil on $x = 180.0$ m begins to liquefy periodically. In each wave period ($T = 10.0$ s), the time status being liquefied is about one third ($1/3$) of the period, rather than half ($1/2$) of the period. Therefore, it is not that the entire seabed under wave trough could liquefy. It is inferred that only $2/3$ of the seabed under wave trough could liquefy. On $x = 180.0$ m, the maximum liquefied depth under the wave loading is

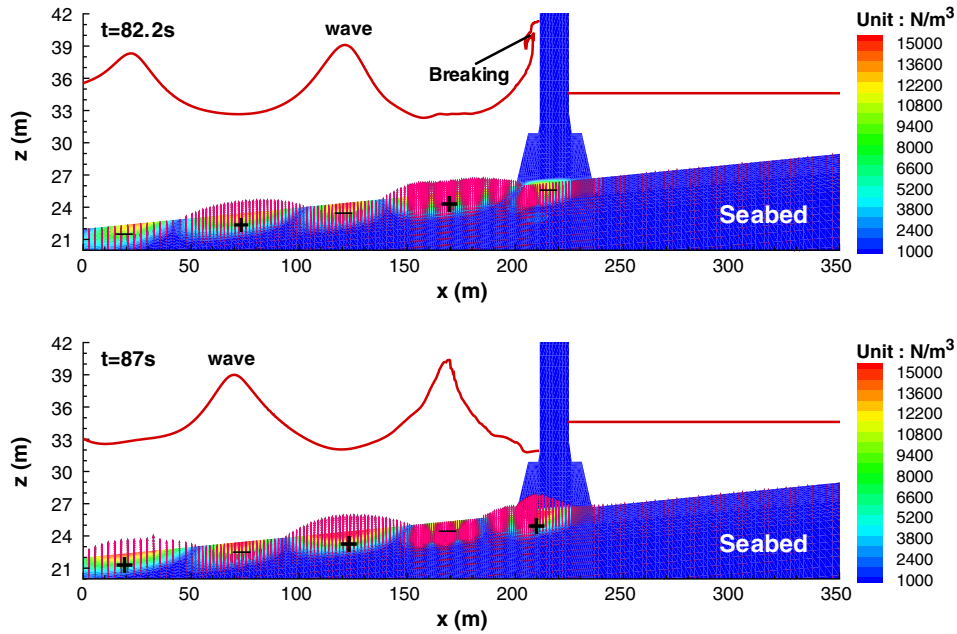


Fig. 13. Seepage force in seabed under the breaking wave loading at $t = 82.2$ s and $t = 87.0$ s. “+”: upward seepage force, “-”: downward seepage force.

about 1.2 m. It is observed from Fig. 15 that the maximum liquefied depth on $x = 180.0$ m decreases gradually with time. The reason would be that the wave energy is dissipated by the composite breakwater.

The wave field in front of the composite breakwater is basically similar with a standing wave due to the interference between the incident wave and the reflected wave. Therefore, the liquefied zone ($x = 150$ m to $x = 200$ m) in front of the composite breakwater will enlarge and shrink periodically. Fig. 16 shows the maximum liquefied depth of the liquefied zone investigated at different times. It can be seen that the maximum liquefied depth is much smaller before the incident wave and reflects wave interference. After the reflected wave and incident wave interfering, the maximum liquefied depth in this liquefied zone increases greatly, and varies periodically. The maximum liquefied depth in the whole computational time domain is about 1.6 m. This potential maximum liquefied depth in the seabed near to marine

structures is an important parameter when designing and managing a marine structure to prevent it from liquefaction induced failure.

How the soil properties and the wave characteristics affect the maximum liquefied depth in the liquefaction zone near to the composite breakwater are important issues. Parametric study is conducted in this paper. Fig. 17 demonstrates the effect of soil properties and wave characteristics on the maximum liquefied depth of the liquefaction zone near to the composite breakwater. As illustrated in Fig. 17, the maximum liquefied depth decreases as the permeability k and the saturation S_r increases. It is also observed that the coarse sand seabed (permeability $k \geq 10^{-3}$ m/s and $S_r = 0.98$) and the fully saturated seabed ($S_r = 1.0$ and $k = 10^{-4}$ m/s) cannot liquefy (transient liquefaction) under wave loading. The shear modulus G of seabed also affects the maximum liquefied depth. The seabed with large stiffness is easier to liquefy transiently under wave loading. Wave height and period are two significant parameters to affect the wave induced maximum

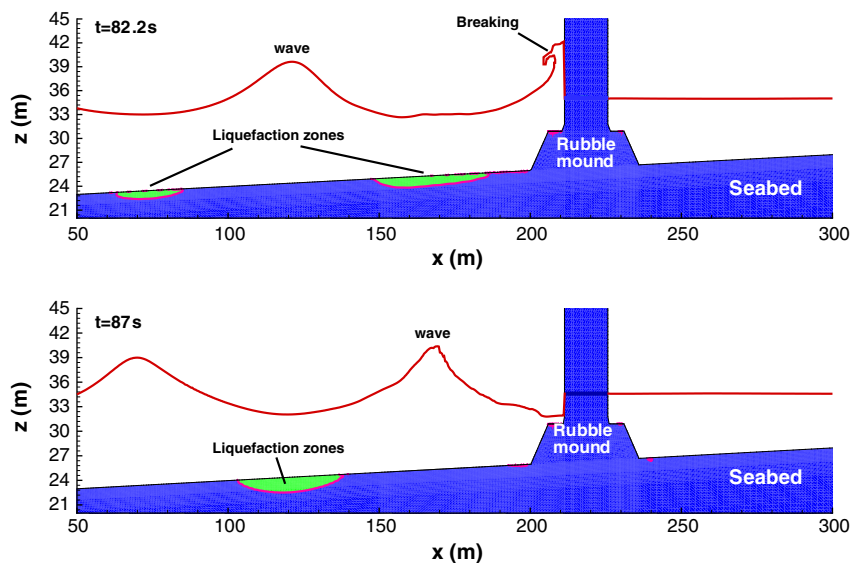


Fig. 14. Predicted liquefaction zones in seabed foundation under the breaking wave loading at typical times $t = 82.2$ s and $t = 87.0$ s.

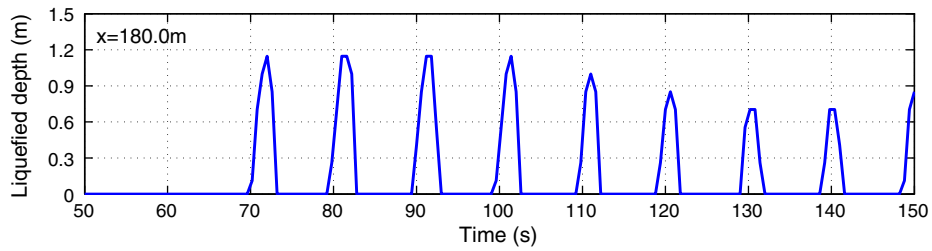


Fig. 15. Liquefied depth on line $x = 180.0$ m in seabed foundation under the breaking wave loading.

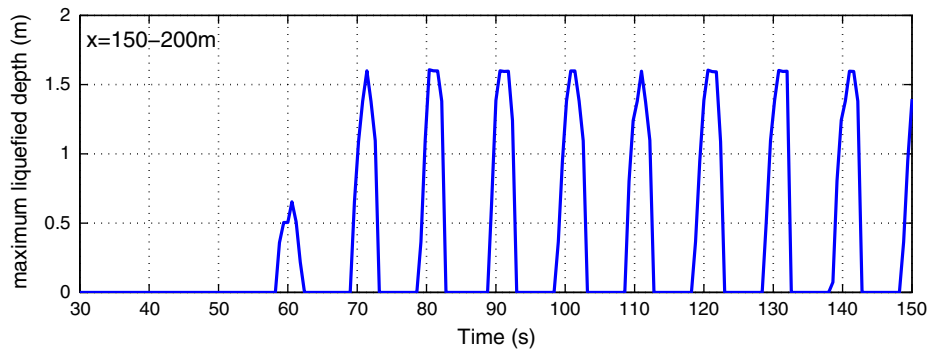


Fig. 16. Maximum liquefied depth of the liquefied zone near to the composite breakwater under the breaking wave loading.

liquefied depth. The maximum liquefied depth in seabed basically has positive correlation with the wave height and wave period, because the wave with large height and period generally carries more wave energy, which will greatly affect the seabed up to a deeper depth.

4. Conclusion

In this study, the interaction between breaking wave, a composite breakwater and its poro-elastic seabed foundation is numerically investigated by adopting the integrated model PORO-WSSI 2D developed by

(Ye, 2012a) and (Jeng et al., 2013). Through analysis, the following conclusion can be draw:

- (1) Under breaking wave loading, the caisson is applied by great impact on its lateral side. When the wave breaks in front of the caisson, correspondingly, the caisson vibrates irregularly; There are series of 'M' shape on the time history curve of horizontal/vertical displacements. The existence of the 'M' shape is attributed to the wave breaking when the wave crest arrives at the breakwater.
- (2) The motion of sea water in front of the composite breakwater is very complicated due to the intensive interaction between the

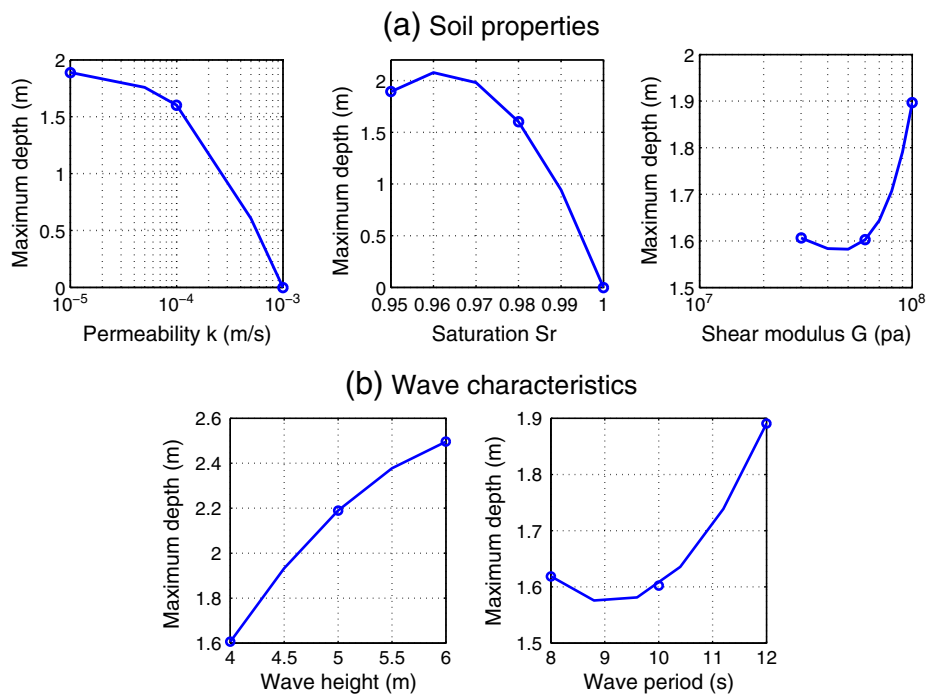


Fig. 17. Effect of soil properties and wave characteristics on the maximum liquefied depth under the breaking wave loading.

wave, seabed foundation and composite breakwater. The turbulence energy of wave in front of the composite breakwater is significant.

- (3) Under the breaking wave loading, the pore pressure, effective stresses in seabed foundation and composite breakwater also vary periodically. Under the wave crest, the dynamic pore pressure is positive, and the dynamic effective stresses are compressive. Under the wave trough, the dynamic pore pressure is negative, and the dynamic effective stresses are tensile.
- (4) A very strong seepage field is generated in the rubble mound, and in the zone near to the seabed surface when the wave propagates on the seabed, and collides with the composite breakwater. Under the wave crest, the seepage force is downward, resulting in the increase of contact effective stresses between soil particles. Under the wave trough, the seepage force is upward, resulting in the decrease of contact effective stresses. When the upward seepage force can overcome the weight of overburdened soil and the composite breakwater, the seabed will liquefy. Numerical analysis indicates that the seabed foundation can liquefy under the breaking wave loading, and the maximum liquefaction depth of the wave-induced transient liquefaction zone in seabed could reach up to 1.6 m.
- (5) The parametric study indicates that the maximum liquefaction depth is positively related to the wave height, wave period and stiffness of seabed soil, and is negatively related to the permeability and saturation of seabed soil.

Acknowledgements

The authors Prof. Wang and Prof. Zhu thank the financial support from Chinese 973 Project: Evolutionary Trends and Sustainable Utilization of Coral Reefs in the South China Sea (2013CB956104). The author Ye Jianhong and Jeng Dongsheng are grateful for the financial support from EPSRC#EP/G006482/1. The author Ye Jianhong also appreciates the funding support of Overseas Research Student Award from Scottish Government, UK.

References

- Biot, M.A., 1941. General theory of three dimensional consolidation. *J. Appl. Phys.* 12 (2), 155–164.
- Biot, M.A., 1956. The theory of propagation of elastic waves in a fluid-saturated porous solid. I. Low-frequency range. *J. Acous. Soc. Am.* 28 (2), 168–178.
- Cha, D.H., Jeng, D.S., Rahman, M.S., Sekiguchi, H., Zen, K., Yamazaki, H., 2002. Effects of dynamic soil behaviour on the wave-induced seabed response. *Int. J. Ocean Eng. Technol.* 16 (5), 21–33.
- Cuomo, G., Allsop, W., Bruce, T., Pearson, J., 2010. Breaking wave loads at vertical seawalls and breakwaters. *Coast. Eng.* 57 (4), 424–439.
- Cuomo, G., Lupoi, G., Shimosako, K., Takahashi, S., 2011a. Dynamic response and sliding distance of composite breakwaters under breaking and non-breaking wave attack. *Coast. Eng.* 58, 953–969.
- Cuomo, G., Piscopia, R., Allsop, W., 2011b. Evaluation of wave impact loads on caisson breakwaters based on joint probability of impact maxima and rise times. *Coast. Eng.* 58 (1), 9–27.
- Hsiao, S.-C., Lin, T.-C., 2010. Tsunami-like solitary waves impinging and overtopping an impermeable seawall: experiment and RANS modelling. *Coast. Eng.* 57 (1), 1–18.
- Hsu, J.R., Jeng, D.S., 1994. Wave-induced soil response in an unsaturated anisotropic seabed of finite thickness. *Int. J. Numer. Anal. Methods Geomech.* 18 (11), 785–807.
- Hsu, T.J., Sakakiyama, T., Liu, P.L.F., 2002. A numerical model for wave motions and turbulence flows in front of a composite breakwater. *Coast. Eng.* 46, 25–C50.
- Huang, C.J., Chang, H.H., Hwung, H.H., 2003. Structural permeability effects on the interaction of a solitary wave and a submerged breakwater. *Coast. Eng.* 49, 1–24.
- Hur, D.S., Kim, C.H., Kim, D.S., Yoon, J.S., 2008. Simulation of the nonlinear dynamic interactions between waves, a submerged breakwater and the seabed. *Ocean Eng.* 35, 511–522.
- Hur, D.S., Kim, C.H., Yoon, J.S., 2010. Numerical study on the interaction among a nonlinear wave, composite breakwater and sandy seabed. *Coast. Eng.* 57 (10), 917–930.
- Jeng, D.S., Hsu, J.R.C., 1996. Wave-induced soil response in a nearly saturated seabed of finite thickness. *Geotechnique* 46 (3), 427–440.
- Jeng, D.S., Cha, D.H., Lin, Y.S., Hu, P.S., 2000. Analysis on pore pressure in an anisotropic seabed in the vicinity of a caisson. *Appl. Ocean Res.* 22, 317–329.
- Jeng, D.S., Cha, D.H., Lin, Y.S., Hu, P.S., 2001. Wave-induced pore pressure around a composite breakwater. *Ocean Eng.* 28, 1413–1435.
- Jeng, D.-S., Ye, J.H., Zhang, J.-S., Liu, P.L.-F., 2013. An integrated model for the wave–seabed–structures interaction – model, verifications and application. *Coast. Eng.* 72 (1), 1–19.
- Lara, J.L., Garcia, N., Losada, I.J., 2006. RANS modeling applied to random wave interaction with submerged permeable structures. *Coast. Eng.* 53, 395–417.
- Lara, J.L., Losada, I.J., Maza, M., Guanche, R., 2011. Breaking solitary wave evolution over a porous underwater step. *Coast. Eng.* 58 (9), 837–850.
- Lin, P., Liu, P.L.F., 1998. A numerical study of breaking waves in the surf zone. *J. Fluid Mech.* 359, 239–264.
- Lin, Z.P., Liu, P.L.-F., 1999. Internal wave-maker for Navier–Stokes equations models. *J. Waterw. Port Coast. Ocean Eng.* 99 (4), 207–215.
- Liu, P.L.F., Lin, P.Z., Chang, K.A., Sakakiyama, T., 1999. Numerical modeling of wave interaction with porous structures. *J. Waterw. Port Coast. Ocean Eng. ASCE* 125, 322–330.
- Madsen, O.S., 1978. Wave-induced pore pressure and effective stresses in a porous bed. *Geotechnique* 28 (4), 377–393.
- Makenna, J.E., 1997. Wave forces on caissons and breakwater crown walls. (PhD thesis) Queen's University of Belfast.
- Mase, H., Sakai, T., Sakamoto, M., 1994. Wave-induced porewater pressure and effective stresses around breakwater. *Ocean Eng.* 21 (4), 361–379.
- Mizutani, N., Mostarfa, A., Iwata, K., 1998. Nonlinear regular wave, submerged breakwater and seabed dynamic interaction. *Coast. Eng.* 33, 177–202.
- Mostafa, A., Mizutani, N., Iwata, K., 1999. Nonlinear wave, composite breakwater, and seabed dynamic interaction. *J. Waterw. Port Coast. Ocean Eng.* 25 (2), 88–97.
- Okusa, S., 1985. Wave-induced stress in unsaturated submarine sediments. *Geotechnique* 35 (4), 517–532.
- Oumeraci, H., Kortenhaus, A., Allsop, N.W.H., de Groot, M.B., Crouch, R.S., Vrijling, J.K., Voortman, H.G., 2001. Probabilistic Design Tools for Vertical Breakwaters. Balkema, Rotterdam.
- Shao, S.H., 2010. Incompressible SPH flow model for wave interactions with porous media. *Coast. Eng.* 57, 304–316.
- Tsai, C.P., 1995. Wave-induced liquefaction potential in a porous seabed in front of a breakwater. *Ocean Eng.* 22 (1), 1–18.
- Tsai, C.P., Lee, T.L., Hsu, J., 2000. Effects of wave nonlinearity on the standing wave-induced seabed response. *Int. J. Numer. Anal. Methods Geomech.* 24, 869–892.
- Ulker, M.B.C., Rahman, M.S., Jeng, D.S., 2009. Wave-induced response of seabed: various formulation and their applicability. *Appl. Ocean Res.* 31, 12–24.
- Ulker, M.B.C., Rahman, M.S., Guddati, M.N., 2010. Wave-induced dynamic response and instability of seabed around caisson breakwater. *Ocean Eng.* 37 (17–18), 1522–1545.
- Ulker, M.B.C., Rahman, M.S., Guddati, M.N., 2012. Breaking wave-induced response and instability of seabed around caisson breakwater. *Int. J. Numer. Anal. Methods Geomech.* 36 (3), 362–390.
- Walkden, M.J.A., Hewson, P.J., Bullock, G.N., 1996. Wave impulse prediction for caisson design. *Proc. of 25th Int. Conf. Coastal Eng., Orlando, Florida, USA. ASCE, New York*, pp. 2584–2597.
- Yamamoto, T., Koning, H., Sellmeijer, H., Hijum, E.V., 1978. On the response of a poro-elastic bed to water waves. *J. Fluid Mech.* 87 (1), 193–206.
- Ye, J.H., 2012a. Numerical Analysis of Wave–Seabed–Breakwater Interactions. (PhD thesis) University of Dundee, Dundee, UK.
- Ye, J.H., 2012b. Numerical modelling of consolidation of 2-D porous unsaturated seabed under a composite breakwater. *Mechanika* 18 (4), 373–379.
- Ye, J.H., Jeng, D.-S., Chan, A.H.C., 2012. Consolidation and dynamics of 3D unsaturated porous seabed under rigid caisson breakwater loaded by hydrostatic pressure and wave. *Science China-Technological Sciences* 55 (8), 2362–2376.
- Ye, J.H., Jeng, D.-S., Wang, R., Zhu, C.Q., 2013. Validation of a 2-D semi-coupled numerical model for fluid-structure-seabed interaction. *Journal of Fluids and Structures* <http://dx.doi.org/10.1016/j.jfluidstructs.2013.04.008> (in press).
- Zienkiewicz, O.C., Chang, C.T., Bettess, P., 1980. Drained, undrained, consolidating and dynamic behaviour assumptions in soils 30 (4), 385–395.